We are IntechOpen, the world's leading publisher of Open Access books Built by scientists, for scientists

4,800
Open access books available

122,000
International authors and editors

135M
Downloads

Our authors are among the

154
Countries delivered to

TOP 1%
most cited scientists

12.2%
Contributors from top 500 universities

CLARIVATE ANALYTICS BOOK CITATION INDEX INDEXED

WEB OF SCIENCE™

Selection of our books indexed in the Book Citation Index in Web of Science™ Core Collection (BKCI)

Interested in publishing with us?
Contact book.department@intechopen.com

Numbers displayed above are based on latest data collected.
For more information visit www.intechopen.com

3

Iron Oxide Nanoparticles

Mohammed M. Rahman[1], Sher Bahadar Khan[1,2],
Aslam Jamal[3], Mohd Faisal[3] and Abdullah M. Aisiri[1,2]
[1]*The Center of Excellence for Advanced Materials Research, King Abdulaziz University, Jeddah*
[2]*Chemistry Department, Faculty of Science, King Abdulaziz University, Jeddah*
[3]*Centre for Advanced Materials and Nano-Engineering (CAMNE),*
Department of Chemistry, Faculty of Sciences and Arts, Najran University, Najran
Kingdom of Saudi Arabia

1. Introduction

A **semiconductor** is a material with electrical conductivity owing to the electron flow (as opposed to ionic conductivity) intermediate in magnitude between that of a conductor and an insulator. This means conductivity roughly in the range of 10^3 to 10^{-8} siemens per centimeter. It is well known that semiconductor has governed a significant role in progressing research in nanoscience and nanotechnology, leading to novel classes of semiconductor nanomaterials which are capable of nano-particles and wide range of synthesis and applications. Semiconductor materials are also the foundation of modern electronics, including radio, computers, telephones, and many other devices. Such devices include transistors, solar cells, many kinds of diodes including the light-emitting diode, the silicon controlled rectifier, and digital and analog integrated circuits. Similarly, semiconductor solar photovoltaic panels directly convert light energy into electrical energy. In a metallic conductor, current is carried by the flow of electrons. In semiconductors, current is often schematized as being carried either by the flow of electrons or by the flow of positively charged "holes" in the electron structure of the material. Actually, however, in both cases only electron movements are involved. Common semiconducting materials are crystalline solids, but amorphous and liquid semiconductors are known. These include hydrogenated amorphous silicon and mixtures of arsenic, selenium and tellurium in a variety of proportions. Such compounds share with better known semiconductors intermediate conductivity and a rapid variation of conductivity with temperature, as well as occasional negative resistance. Such disordered materials lack the rigid crystalline structure of conventional semiconductors such as silicon and are generally used in thin film structures, which are less demanding for as concerns the electronic quality of the material and thus are relatively insensitive to impurities and radiation damage. Organic semiconductors, that is, organic materials with properties resembling conventional semiconductors, are also known. Silicon is used to create most semiconductors commercially. Dozens of other materials are used, including germanium, gallium arsenide, and silicon carbide. A pure semiconductor is often called an “intrinsic” semiconductor. The electronic properties and the conductivity of a semiconductor can be changed in a controlled manner by adding very small quantities of other elements, called “dopants”, to the intrinsic material. In crystalline silicon typically this is achieved by adding impurities of boron or phosphorus to the melt and then allowing the melt to solidify into the crystal.

An iron oxide nanoparticle, in nanotechnology, a particle is defined as a small object that behaves as a whole unit in terms of its transport and properties. Particles are further classified according to size: in terms of diameter, fine particles cover a range between 100 and 2500 nanometers. On the other hand, ultrafine particles are sized between 1 and 100 nanometers. Similar to ultrafine particles, nanoparticles are sized between 1 and 100 nanometers. Nanoparticles may or may not exhibit size-related properties that differ significantly from those observed in fine particles or bulk materials (Buzea et al., 2007). Although the size of most molecules would fit into the above outline, individual molecules are usually not referred to as nanoparticles. Nanoclusters have at least one dimension between 1 and 10 nanometers and a narrow size distribution. Nanopowders (Fahlman, 2007) are agglomerates of ultrafine particles, nanoparticles, or nanoclusters. Nanometer-sized single crystals, or single-domain ultrafine particles, are often referred to as nanocrystals. Nanoparticle research is currently an area of intense scientific interest due to a wide variety of potential applications in biomedical, optical and electronic fields.

Iron oxides are chemical compounds composed of iron and oxygen. Altogether, there are sixteen known iron oxides and oxyhydroxides (Cornell & Schwertmann, 2003). The uses of these various oxides and hydroxides are tremendously diverse ranging from pigments in ceramic glaze, to use in thermite.

Oxides:

- iron(II) oxide, wüstite (FeO)
- iron(II,III) oxide, magnetite (Fe_3O_4)
- iron(III) oxide (Fe_2O_3)
  - alpha phase, hematite (α-Fe_2O_3)
  - beta phase, (β-Fe_2O_3)
  - gamma phase, maghemite (γ-Fe_2O_3)
  - epsilon phase, (ε-Fe_2O_3)

Hydroxides:

- iron(II) hydroxide ($Fe(OH)_2$)
- iron(III) hydroxide ($Fe(OH)_3$), (bernalite)

Oxide/hydroxide:

- goethite (α-FeOOH),
- akaganéite (β-FeOOH),
- lepidocrocite (γ-FeOOH),
- feroxyhyte (δ-FeOOH),
- ferrihydrite ($Fe_5HO_8 \cdot 4H_2O$ approx.), or $5Fe_2O_3.9H_2O$, better recast as $FeOOH.0.4H_2O$
- high-pressure FeOOH
- schwertmannite (ideally $Fe_8O_8(OH)_6(SO) \cdot nH_2O$ or $Fe^{3+}{}_{16}O_{16}(OH,SO_4)_{12\text{-}13} \cdot 10\text{-}12H_2O$)

Beta phase iron oxide: Cubic face centered, metastable, at temperatures above 500 °C converts to alpha phase. It can be prepared by reduction of hematite by carbon, pyrolysis of iron(III) chloride solution, or thermal decomposition of iron(III) sulfate.

Iron(III) oxide or **ferric oxide** is the inorganic compound with the formula Fe_2O_3. It is of one of the three main oxides of iron, the other two being iron(II) oxide (FeO), which is rare, and iron(II,III) oxide (Fe_3O_4), which also occurs naturally as the mineral magnetite. As the mineral known as hematite, Fe_2O_3 is the main source of the iron for the steel industry. Fe_2O_3 is paramagnetic, reddish brown, and readily attacked by acids. Rust is often called iron(III) oxide, and to some extent, this label is useful, because rust shares several properties and has a similar composition. To a chemist, rust is considered an ill-defined material, described as hydrated ferric oxide.

2. Literature survey

Semiconducting nano-materials have attracted much attention because of their unique properties and potential applications in all areas of science (Kumar & Singhal, 2007). The simplest synthetic route to nanomaterials is probably self aggregation, in which ordered aggregates are formed in a spontaneous process (Whitesides & Boncheva, 2002). However, it is still a big challenge to develop simple and reliable synthetic way for low-dimensional metal oxide nanostructures with designed chemical components and controlled morphologies which strongly affect the properties of nano-materials (Dale & Huber, 2009). In recent years, nanosized and nanostructures of super-paramagnetic iron oxides have been investigated extensively because of their wide applications in nano-fields such as ferro-fluids (Raj et al., 1995), magnetocaloric refrigeration (McMichael et al., 1992), biotechnology, and in vivo bio-medical field (Rahman et al., 2011). These materials offer several potential biomaterial (Rahman et al., 2011) as well as biomedical (Rahman et al., 2009) applications in magnetically controlled drug delivery, magnetic resonance imaging as contrast agent, tissue repair, and detoxification of biological fluids (Garcia et al., 2004; Music et al., 1997). It has been extensively studied in diverse fields including catalysis (Brown et al., 1998) environment protection (Chen et al., 2005), magnetic storage media (Zeng et al., 2002), clinical diagnosis, and treatment (Jordan et al., 2003). Nanomaterials may also be utilized in different technological requests, viz. refrigeration systems, medical imaging, drug targeting, other biological applications, and catalysis (Kesavan et al., 1999). Reducing the crystal dimension and enhancing the surface area of the sensing materials are an optional approach to improve the responses, since the reduction/oxidation reactions are mainly activated by the active surfaces area.

Removal of organic pollutants (especially AO dye) in water has been a significant issue in wastewater treatment because of the non-biodegradable nature of these pollutants. The degradation methods, such as, adsorption using activated carbon and coagulation using coagulants, actively convert the aqueous dyes to the solid state leaving the contaminant intact. During the past decades, many researchers have put focus on searching for a direct and effective method to solve this problem (Rahman et al., 2006; Saquib et al., 2008). Recently the ecological contamination and inadvertent leakage of detrimental gases and liquids, semiconducting metal oxide chemical sensors have attracted the interest of ecologists, technologists, environmentalist, and others (Pare et al., 2008). One of the industrial gases in liquid form of interest is ammonia as an ammonium hydroxide because of its toxic and polluting nature. Because of its wide variety of applications including the production of nitrogenous fertilizers and other nitrogenous chemicals, as well as an industrial refrigerant, its global production is in excess of 100 million tons per annum. If highly concentrated it might lead to severe burns on our skin, eyes, throat, or lungs causing permanent blindness and lung disease. In addition, ammonia, hydroxide aerosols have a sun blocking function, corrosive natures, and the fume produced results in temperature reduction. Hence early detection and monitoring of presence of ammonium hydroxide in a wide range of industrial applications is desired. Solution phase ammonia sensors based on optical, electrical, and chemical detection have focused significant attention due to the possibility to operate at room temperature, to measure low level concentrations with fast response time and applicable to detect trace level ammonia solution in environments. In order to detect NH_4OH, there have been lots of efforts in developing a variety of chemical sensors such as electrochemical sensor and chemi-resistive sensors (Ballun et al., 2003), and optical sensors (Christie et al., 2003).

Many sensing research works have been performed with the metal oxide nanostructures for the detection of various chemicals such as hydrazine, acetone, ethanol etc. The chemical sensing by metal oxide thin films utilize mainly the properties of thin film formed by the physi-sorption and chemisorptions techniques. The chemical detection is based on the current changes of the fabricated thin films caused by the chemical components of the reacting system in aqueous medium (Ansari et al., 2008). Here, the main efforts are focused on detecting the minimum ammonium hydroxide concentration necessary for electrochemical detection. Low-dimension of NPs in metal oxide nanostructures allows very sensitive transduction of the liquid/surface interactions into a change in the electrochemical properties. The possibility to form a variety of structural morphologies metal oxide NPs offers many opportunities of tuning the chemical sensing properties. Taking into account their applications, low-dimensional NPs with iron oxide is prepared by hydrothermal technique to fabricate a simple and efficient chemical sensors consisting on a side-polished gold surface; and to test the chemical sensing performance on ammonium hydroxide at room temperature. To best of our knowledge, this is the first report for detection of ammonium hydroxide (in liquid phase) using simple and reliable I-V technique in short response time. Additionally we investigated the photo-catalytic degradation of organic dye named AO (water soluble) with as-grown iron oxide NPs in aqueous system under 250W mercury lamp.

3. Experimental sections

3.1 Materials and methods

Ferric chloride, urea, ammonia solution (25%), acridine orange, butyl carbitol acetate, ethyl acetate, monosodium phosphate, disodium phosphate, and all other chemicals used were of analytical grade and purchased from Sigma-Aldrich Company. The λ_{max} (404 nm) of as-grown Iron particles was measured using UV/visible spectroscopy Lamda-950, Perkin Elmer, Germany. FT-IR spectra were recorded on a Spectrum-100 FT-IR spectrophotometer in the mid-IR range in KBr media purchased from Perkin Elmer, Germany. Raman station 400 was used to measure the Raman shift of as-grown iron NPs using radiation source (Ar^+ laser line, λ; 513.4 nm), which was purchased from Perkin Elmer, Germany. Morphology of iron oxide NPs were recorded on FE-SEM instrument (FESEM; JSM-7600F, Japan). Elemental analysis was investigated using EDS from JEOL, Japan. The morphologies, sizes, and structures of NPs were executed by HR-TEM (TEM; JEM-2100F, Japan). HR-TEM sample were prepared as follows; the synthesized as-grown iron NPs were dispersed into ethanol under ultrasonic vibration for 5 minutes. Then the HR-TEM film is dipped in the solution and dry for investigation. The powder X-ray diffraction (XRD) patterns were taken on a X-ray diffractometer (XRD; X'Pert Explorer, PANalytical diffractometer) equipped with Cu-$K\alpha_1$ radiation (λ =1.5406 nm) using a generator voltage of 45 kV and a generator current of 40 mA were applied for the determination. I-V technique is employed by using Electrometer (Kethley, 6517A, Electrometer, USA).

3.2 Hydrothermal methods

Hydrothermal synthesis includes the various techniques of crystallizing substances from high-temperature aqueous solutions at high vapor pressures; also termed "hydrothermal method". The term "hydrothermal" is of geologic origin. Geochemists and mineralogists have studied hydrothermal phase equilibria since the beginning of the twentieth century.

George W. Morey at the Carnegie Institution and later, Percy W. Bridgman at Harvard University did much of the work to lay the foundations necessary to containment of reactive media in the temperature and pressure range where most of the hydrothermal work is conducted. Hydrothermal synthesis can be defined as a method of synthesis of single crystals that depends on the solubility of minerals in hot water under high pressure. The crystal growth is performed in an apparatus consisting of a steel pressure vessel called autoclave, in which a nutrient is supplied along with water. A gradient of temperature is maintained at the opposite ends of the growth chamber so that the hotter end dissolves the nutrient and the cooler end causes seeds to take additional growth. Possible advantages of the hydrothermal method over other types of crystal growth include the ability to create crystalline phases which are not stable at the melting point. Also, materials which have a high vapor pressure near their melting points can also be grown by the hydrothermal method. The method is also particularly suitable for the growth of large good-quality crystals while maintaining good control over their composition. Disadvantages of the method include the need of expensive autoclaves, and the impossibility of observing the crystal as it grows (O'Donoghue, 1983). A large number of compounds belonging to practically all classes have been synthesized under hydrothermal conditions: elements, simple and complex oxides, tungstates, molybdates, carbonates, silicates, germanates etc. Hydrothermal synthesis is commonly used to grow synthetic quartz, gems and other single crystals with commercial value. Some of the crystals that have been efficiently grown are emeralds, rubies, quartz, alexandrite and others. The method has proved to be extremely efficient both in the search for new compounds with specific physical properties and in the systematic physicochemical investigation of intricate multicomponent systems at elevated temperatures and pressures.

3.3 Synthesis of Iron oxide NPs

Low dimensional iron oxide NPs have been synthesized by adding uni-molar concentration of ferric chloride and urea into hydrothermal cell (Teflon line autoclave). $FeCl_3$ and urea were slowly dissolved into the de-ionized water separately to make 0.5 M concentration at room temperature. Then the solution was mixed gently and stirred until mix properly. The solution pH was slowly adjusted using ammonia solution drop wise to approximately 9.66. Then the mixture was put in hydrothermal cell (Teflon line autoclave) to put in the oven for 6 hours heated up and maintained at 150^{o}C. Then the solution was washed with acetone and kept for drying at room temperature. The as-grown iron oxide products were characterized in detail in terms of their structural and optical properties.

The development of Fe_2O_3 nanoparticles can be well explained stranded on the chemical reactions concerned and crystal growth behaviors of iron oxide. For the synthesis of Fe_2O_3 NPs, ferric chloride ($FeCl_3$) and NH_4OH (in presence of urea) were mixed under continuous stirring at 150^{o}C. During the reaction method, the NH_4OH performs in major rules, like control the pH value of the solution as well as resource to supply hydroxyl ions to the solution. The $FeCl_3$ reacts with NH_4OH and forms FeOOH, which, upon heating, further produce into Fe^{2+} and OH^- ions, which consequently assists in the development of Fe_2O_3 ions according to the chemical reactions **(i)-(iii)**.

$$NH_4OH_{(aq)} \rightarrow NH_4^+{}_{(aq)} + OH^-{}_{(aq)} \quad \text{(i)}$$

$$FeCl_{3(s)} \rightarrow Fe^{2+}{}_{(aq)} + 3Cl^-{}_{(aq)} \quad \text{(ii)}$$

$$Fe^{2+}_{(aq)} + 2OH^{-}_{(aq)} \rightarrow FeOOH_{(aq)} + H^{+} \quad \text{(iii)}$$

The FeOOH finally, however dissociates to the formation of Fe_2O_3 nuclei according to the reactions **(iv)-(v).**

$$FeCl_{3(aq)} + 2NH_4OH_{(aq)} \rightarrow FeOOH_{(aq)} + 2NH_4^{+}{}_{(aq)} + H^{+}_{(aq)} + 3Cl^{-}_{(aq)} \quad \text{(iv)}$$

$$FeOOH_{(aq)} \rightarrow Fe_2O_{3(s)} + H_2O_{(l)} \quad \text{(v)}$$

The initially formed Fe_2O_3 nuclei perform as building blocks for the development of final products. With reaction time under the appropriate heating conditions in hydrothermal method, the Fe_2O_3 nuclei concentration enlarges which escorts the construction of desired nanoparticle products. As the Fe_2O_3 NPs are prepared by the well accretion of low-dimensional particles, therefore it is supposed that the fundamental entity for the configuration of Fe_2O_3 structure is nanoparticles.

3.4 Photocatalyst

In chemistry, photocatalysis is the acceleration of a photoreaction in the presence of a catalyst. In catalyzed photolysis, light is absorbed by an adsorbed substrate. In photogenerated catalysis, the photocatalytic activity (PCA) depends on the ability of the catalyst to create electron–hole pairs, which generate free radicals (hydroxyl radicals: OH) able to undergo secondary reactions. Its comprehension has been made possible ever since the discovery of water electrolysis by means of the titanium dioxide. Commercial application of the process is called advanced oxidation process (AOP). There are several methods of achieving AOP's that can but do not necessarily involve TiO_2 or even the use of UV light. Generally the defining factor is the production and use of the hydroxyl radical.

3.5 Photocatalytic degradation of AO with NPs

Photo-catalytic degradation of AO using Iron oxide NPs was executed by optical absorption spectroscopy. The catalytic reaction was carried out in a 250.0 ml beaker, which contain 150.0 ml of AO dye solution (0.03 mM) and 150.0 mg of catalyst. Prior to irradiation, the solution was stirred and bubbled with oxygen for at least 15 min in the dark to allow equilibrium of the system so that loss of compound owing to the adsorption can be taken into account. The suspension was continuously purged with oxygen bubbling throughout the experiment. Irradiation was carried out using 250 W Mercury lamps. Samples (5.0 ml) were composed before and at usual intervals during the irradiation and AO solution were isolated from the photo-catalyst by centrifugation before analysis. The degradation was investigated by measuring the absorbance using UV-visible spectrophotometer (Lambda 950). The absorbance of AO (0.03 mM) was followed at 491 nm wavelength. All solutions were prepared and organized with de-ionized water in room conditions.

3.6 Fabrication of gold electrode using NPs

Gold electrode (surface area 0.0216 cm^2) is fabricated with as-grown iron NPs where butyl carbitol acetate (BCA) and ethyl acetate (EA) as a fabricating agent. Then it is kept in the oven at 50^{o}C for 2 hours until the film is completely uniform, stable, and dried. Phosphate buffer solution (PBS, 0.1M, pH 7.0) is prepared by mixing 0.2M Na_2HPO_4 and 0.2M NaH_2PO_4 solution in 100.0ml de-ionize water. The as-grown iron oxide NPs were employed

for the detection of ammonia in liquid phase. The thin film of NPs were made with conducting binders and embedded on the gold electrode, which is presented in the Scheme 1. The Pd and gold electrodes are used as counter and working electrodes, which are presented in Scheme 1A and Scheme 1B respectively. The fabricated electrode was kept in the oven at low temperature (60.0^{o}C) for 2 hours to dry and uniform the film completely (Scheme 1B). The ammonium hydroxide was used as a target chemical in the liquid phase for the total measurement. The electrical response of target compound has been measured using I-V method, which is shown in Scheme 1C.

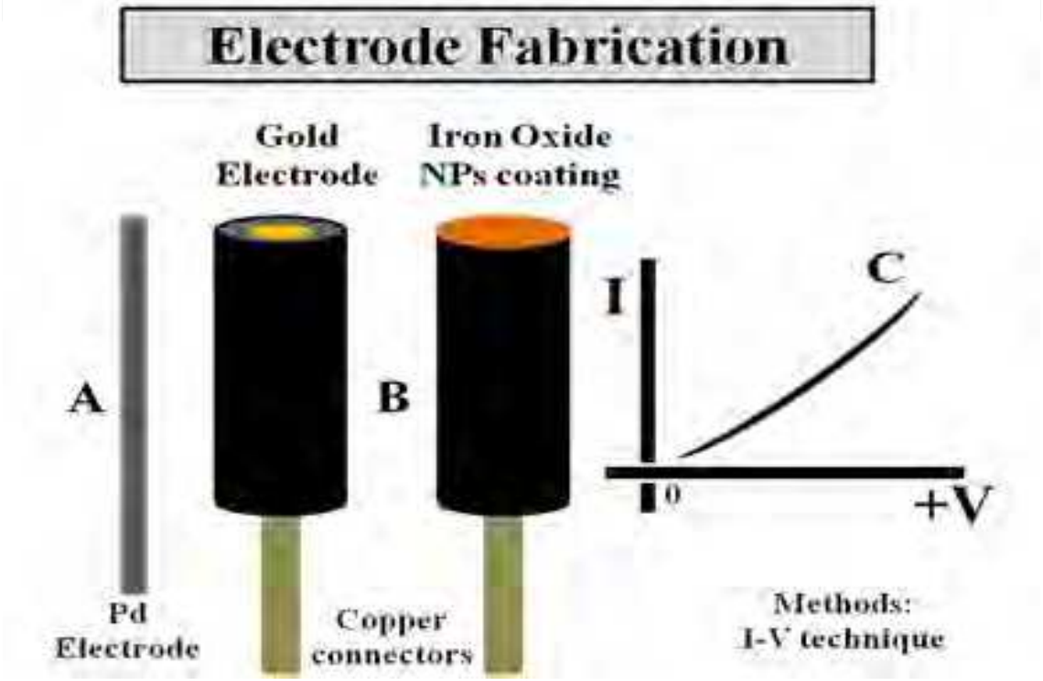

Scheme 1. Fabrication of chemical sensors using as-grown β-Fe_2O_3 NPs and its detection methodology

3.7 Lower detection limit (LOD)

In analytical chemistry, the **detection limit**, lower limit of detection, or **LOD** (limit of detection), is the lowest quantity of a substance that can be distinguished from the absence of that substance (a blank value) within a stated confidence limit (generally 1%) (MacDougall & Crummett, 1980). The detection limit is estimated from the mean of the blank, the standard deviation of the blank and some confidence factor. Another consideration that affects the detection limit is the accuracy of the model used to predict concentration from the raw analytical signal. There are a number of different "detection limits" that are commonly used. These include the instrument detection limit (IDL), the method detection limit (MDL), the practical quantification limit (PQL), and the limit of quantification (LOQ). Even when the same terminology is used, there can be differences in the LOD according to nuances of what definition is used and what type of noise contributes to the measurement and calibration (Long & Winefordner, 1983).

3.8 Linear dynamic range (LDR)

The detector response is said to be linear if the difference in response for two concentrations of a given compound is proportional to the difference in concentration of the two samples. Such response appears as a straight line in the calibration curve. The linear dynamic range of a detector is the maximum linear response divided by the detector noise. Most detectors eventually become non-linear as sample size is increased and this upper point is usually well defined. The chromatographer should know where this occurs to avoid errors in quantification.

3.9 Detection of ammonium hydroxide by I-V technique

A cell is constructed consisting of NPs coated gold electrode as a working electrode and Pd wire is used a counter electrode. Ammonium hydroxide solution is diluted at different concentrations in DI water and used as a target chemical. Amount of 0.1M phosphate buffer solution was kept constant as 20.0 ml throughout the investigation. Solution is prepared with various concentrations of ammonium hydroxide as 77.0 μM to 7.7 M (25% ammonia solution). The sensitivity is calculated from the ratio of voltage versus current of the calibration plot. Electrometer is used as a voltage sources for I-V measurement in simple two electrode system.

4. Properties of nanoparticles

4.1 Optical properties of β-Fe_2O_3 NPs

The optical property of the β-Fe_2O_3 nanoparticles is one of the important characteristics for the evaluation of its optical and photocatalytic activity. UV/visible absorption are a method in which the outer electrons of atoms or molecules absorb radiant energy and undergo transitions to high energy levels. In this procedure, the spectrum obtained owing to optical absorption can be analyzed to acquire the energy band gap of the semiconductor nanomaterials. The optical absorption measurement was carried out at room conditions. Therefore, the nanomaterial may be helpful for the development of non-linear optical sensors in this wavelength region, as the lack of absorption peaks is the major prerequisite for the nanomaterials to confirm non-linear properties. The absorption spectrum of as-grown iron oxide NPs solution is presented in **Fig. 1**(A). It displays an onset of absorption maxima at 404.0 nm in visible range between 200 to 800 nm wavelengths. The lambda maxima of as grown NPs are quite different to those observed earlier due to α-Fe_2O_3 and γ -Fe_2O_3 (Cherepy et al., 1998) but are very similar to those reported for β-Fe_2O_3 (Cornell & Schwertmann, 2003). It shows a broad absorption band around 404.0 nm indicating the formation of low dimensional β-Fe_2O_3 NPs having reddish colors. Band gap energy is calculated on the basis of the maximum absorption band (404nm) of β-Fe_2O_3 NPs and obtained to be 3.06931 eV, according to following equation (vi).

$$E_{bg} = \frac{1240}{\lambda}(\text{eV}) \tag{vi}$$

Where E_{bg} is the band-gap energy and λ_{max} is the wavelength (404.0 nm) of the nanoparticles.

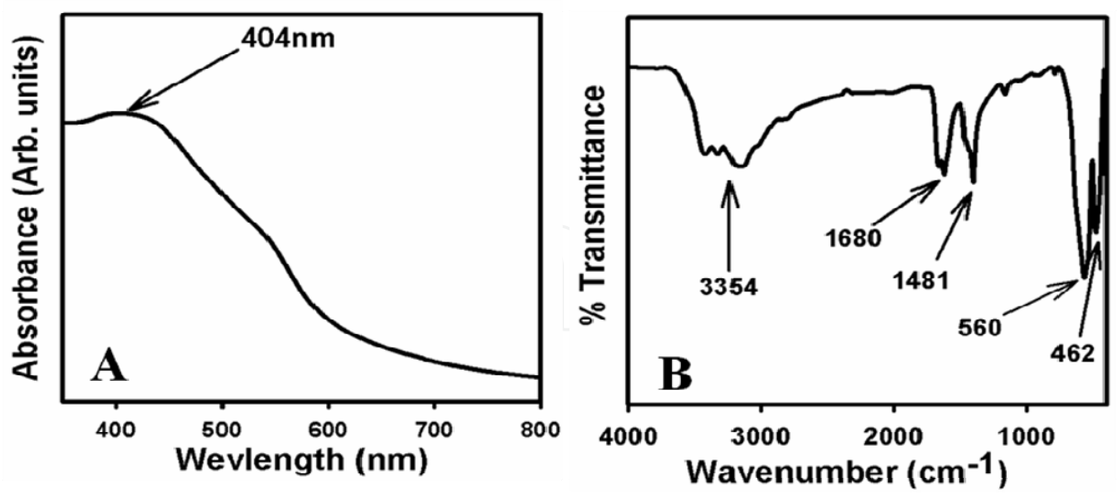

Fig. 1. (A) UV-vis absorption and (B) FT-IR spectra of as-grown Fe_2O_3 NPs.

Infrared spectroscopy (IR spectroscopy) is the spectroscopy that deals with the infrared region of the electromagnetic spectrum that is light with a longer wavelength and lower frequency than visible light. It covers a range of techniques, mostly based on absorption spectroscopy. As with all spectroscopic techniques, it can be used to identify and study chemicals. A common laboratory instrument that uses this technique is a Fourier transform infrared (FT-IR) spectrometer. The infrared portion of the electromagnetic spectrum is usually divided into three regions; the near-, mid- and far- infrared, named for their relation to the visible spectrum. The higher energy near-IR, approximately 14000–4000 cm^{-1} (0.8–2.5 µm wavelength) can excite overtone or harmonic vibrations. The mid-infrared, approximately 4000–400 cm^{-1} (2.5–25 µm) may be used to study the fundamental vibrations and associated rotational-vibrational structure [**Fig. 2**]. The far-infrared, approximately 400–10 cm^{-1} (25–1000 µm), lying adjacent to the microwave region, has low energy and may be used for rotational spectroscopy. The names and classifications of these subregions are conventions, and are only loosely based on the relative molecular or electromagnetic properties. **Fourier transform infrared (FT-IR)** spectroscopy is a measurement technique that allows one to record infrared spectra. Infrared light is guided through an interferometer and then through the sample (or vice versa). A moving mirror inside the apparatus alters the distribution of infrared light that passes through the interferometer. The signal directly recorded, called an "interferogram", represents light output as a function of mirror position. A data-processing technique called Fourier transform turns this raw data into the desired result (the sample's spectrum): Light output as a function of infrared wavelength (or equivalently, wavenumber). There is an alternate method for taking spectra (the "dispersive" or "scanning monochromator" method), where one wavelength at a time passes through the sample. The dispersive method is more common in UV-Vis spectroscopy, but is less practical in the infrared than the FTIR method. One reason that FTIR is favored is called "Fellgett's advantage" or the "multiplex advantage": The information at all frequencies is collected simultaneously, improving both speed and signal-to-noise ratio. Another is called "Jacquinot's Throughput Advantage": A dispersive measurement requires detecting much lower light levels than an FTIR measurement. There are other advantages, as well as some disadvantages, but virtually all modern infrared spectrometers are FTIR instruments.

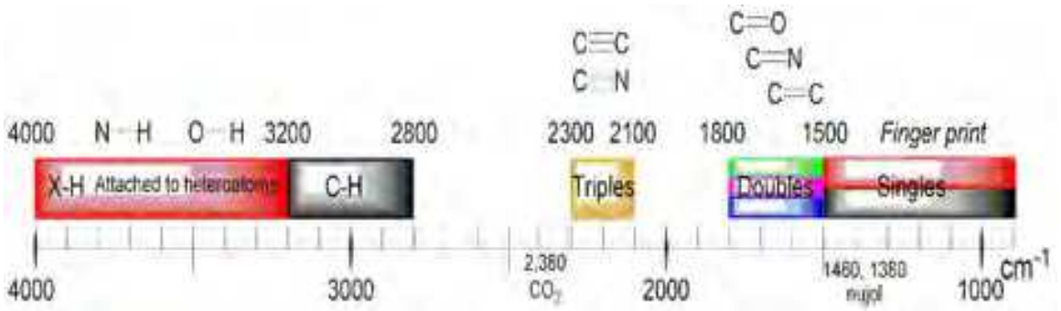

Fig. 2. FT-IR wave range for fundamental vibrations and associated rotational-vibrational frequencies

Fig. 1(B) represents the FT-IR spectrum of the as- grown NPs. It displays several bands at 462, 560, 1481, 1680, and 3354 cm^{-1}. The observed vibration bands may be assigned to Fe–O–Fe stretching vibration (462 and 560 cm^{-1}), O=C=O stretching vibration (1481 cm^{-1}), O-H stretching (3354 cm^{-1}), and O-H bending vibration (1680 cm^{-1}). The absorption bands at 1481, 1680, and 3354 cm^{-1} normally comes from carbon dioxide and water which generally nanomaterials absorbed from the environment due to their mesophorous structure. The observed vibration bands at low frequencies regions suggest the formation of β-Fe_2O_3.

4.2 Structural properties of of β-Fe_2O_3 NPs

Raman spectroscopy is a spectroscopic method utilized to reveal vibrational, rotational, and other low-frequency phases in a Raman active compounds. It depends on inelastic scattering, or Raman scattering, of monochromatic light, generally from a laser in the visible, near infrared, or near ultraviolet range [**Fig. 3**]. The laser light communicates with molecular vibrations, phonons or other excitations in the modes, showing in the energy of the laser photons being shifted up or down. The shift in energy represents information regarding the phonon modes in the system, where Infrared spectroscopy yields similar, but complementary information. Raman spectroscopy is generally established and utilized in material chemistry, since the information is specific to the chemical bonds and symmetry of metal-oxygen stretching or vibrational modes.

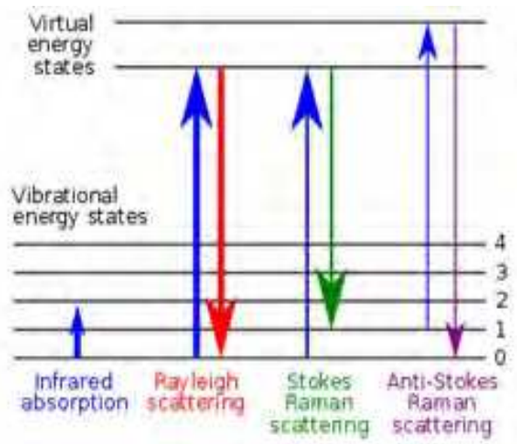

Fig. 3. Energy level diagram showing the states involved in Raman signal. The line thickness is roughly proportional to the signal strength from the different transitions.

Fig. 4A shows the Raman spectrum where main features of the wave-number are observed at about 221, 290, 410, 500, and 608 cm^{-1} for Fe-O stretching vibration. These large bands may be assigned to a magnetite phase of iron oxide NPs. At 608 cm^{-1}, higher wave-number shift is observed due to the various dimensional effects of the NPs.

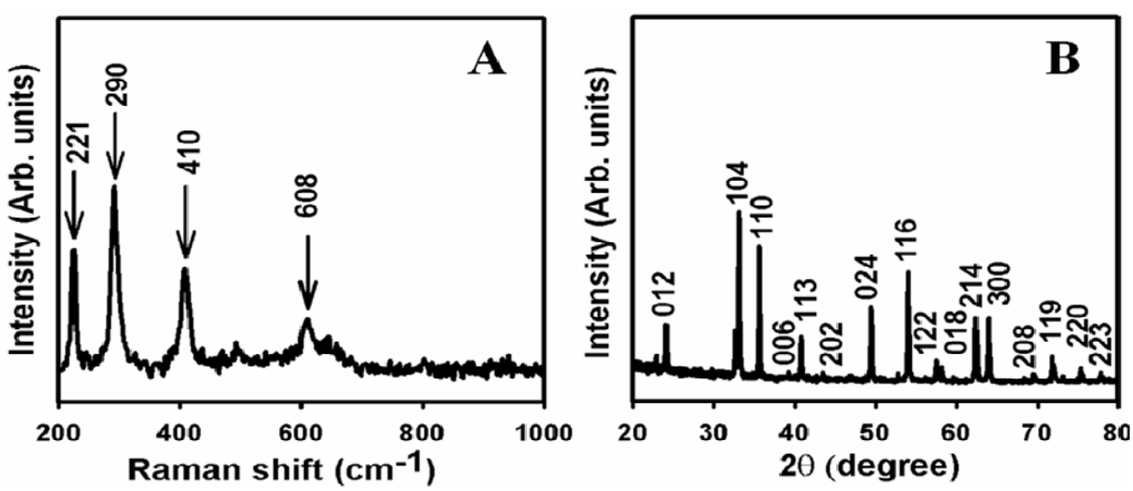

Fig. 4. (A) Raman spectra and (B) XRD patterns of as-grown iron oxide NPs.

X-ray scattering techniques are a family of non-destructive analytical techniques which reveal information about the crystallographic structure, chemical composition, and physical properties of materials and thin films. These techniques are based on observing the scattered intensity of an X-ray beam hitting a sample as a function of incident and scattered angle, polarization, and wavelength or energy. X-ray diffraction yields the atomic structure of materials and is based on the elastic scattering of X-rays from the electron clouds of the individual atoms in the system. The most comprehensive description of scattering from crystals is given by the dynamical theory of diffraction (Azároff et al., 1974). X-ray diffraction can be used to determine which iron oxide compounds are present in NPs by calculating or comparing with the standard value of lattice parameters, crystal structures and crystallinity. **Fig. 4**B shows typical crystallinity of the synthesized as-grown iron oxide NPs and their aggregates. All the reflection peaks in this pattern were found to match with the β-Fe_2O_3 phase having rhombohedral geometry [JCPDF # 089-2810]. The lattice parameters are a = 5.04, c = 13.75, point group: R-3c, and Radiation: CuKα1 (λ= 1.5406). The sample showed the major characteristic peaks for as grown crystalline metallic iron at 2θ values of 24.2(012), 32.2(104), 35.7(110), 39.4(006), 40.9(113), 43.5(202), 49.5(024), 54.1(116), 57.3(122), 57.6(018), 62.5(214), 64.0(300), 69.6(208), 72.0(119), 75.4(220), and 78.0(223) degrees. These indicate that the as-grown iron oxide NPs is well crystalline β-Fe_2O_3.

As scanning electron microscopes (SEM) have evolved the electron beam cross section has become smaller and smaller increasing magnification several fold. A field-emission cathode in the electron gun of a scanning electron microscope provides narrower probing beams at low as well as high electron energy, resulting in both improved spatial resolution and minimized sample charging and damage. Advantages of SEM are (a) semiconductor device cross section analyses for gate widths, gate oxides, film thicknesses, and construction details, (b) advanced coating thickness and structure uniformity determination, and (c) small contamination feature geometry and elemental composition measurement. High resolution

FE-SEM images of as-grown low dimensional iron oxide NPs are presented in Figure 5. Figure 5A to 5E shows the low to high magnified images of NPs grown by hydrothermal process. It is clear from the FE-SEM images that the synthesized products are NPs, which grown in a very high-density and possessed almost uniform shape presented in Figure 5A to 5D. Figure 5E exhibits the high-resolution FE-SEM image of the synthesized NPs which reflected that most of the NPs possessing spherical shapes. The diameter of iron NPs is calculated in the range of 50-90 nm where the average diameter of iron oxide NPs is close to 60 ± 10 nm.

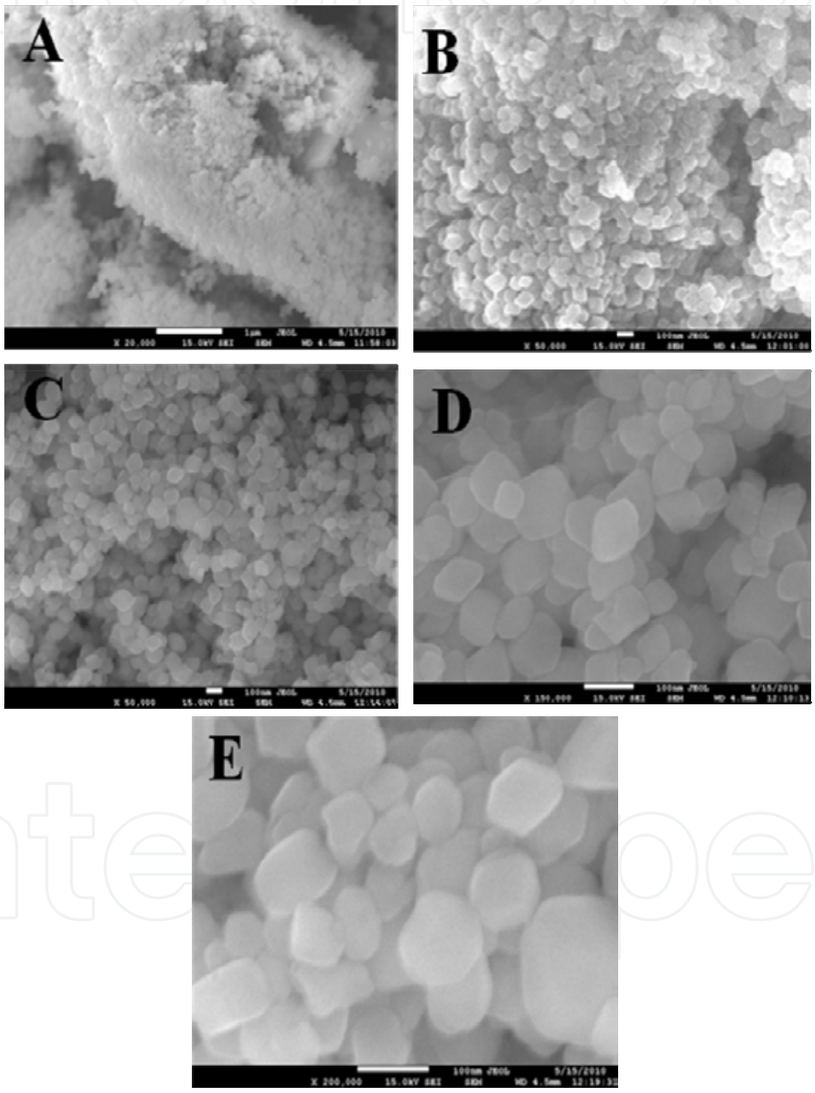

Fig. 5. (A)-(E) Low to High resolution FE-SEM images of as-grown iron oxide NPs

Energy-dispersive X-ray spectroscopy (EDS or EDX) is an analytical technique used for the elemental analysis or chemical characterization of a sample. It is one of the variants of X-ray fluorescence spectroscopy which relies on the investigation of a sample through interactions between electromagnetic radiation and matter, analyzing X-rays emitted by the matter in

response to being hit with charged particles. Its characterization capabilities are due in large part to the fundamental principle that each element has a unique atomic structure allowing X-rays that are characteristic of an element's atomic structure to be identified uniquely from one another. To stimulate the emission of characteristic X-rays from a specimen, a high-energy beam of charged particles such as electrons or protons or a beam of X-rays, is focused into the sample being studied. At rest, an atom within the sample contains ground state (or unexcited) electrons in discrete energy levels or electron shells bound to the nucleus. The incident beam may excite an electron in an inner shell, ejecting it from the shell while creating an electron hole where the electron was. An electron from an outer, higher-energy shell then fills the hole, and the difference in energy between the higher-energy shell and the lower energy shell may be released in the form of an X-ray. The number and energy of the X-rays emitted from a specimen can be measured by an energy-dispersive spectrometer. As the energy of the X-rays is characteristic of the difference in energy between the two shells, and of the atomic structure of the element from which they were emitted, this allows the elemental composition of the specimen to be measured. The electron dispersive spectroscopy (EDS) analysis of these particles indicates the presence of Fe and O composition in the pure as-grown iron oxide NPs (Fe_2O_3). It is clearly displayed that as-grown synthesize materials contained only iron and oxygen elements, which presented in **Fig. 6**. The composition of iron and oxygen is 54.11% and 45.88% respectively. No other peak related with any impurity has been detected in the EDS, which confirms that the as-grown NPs are composed only with iron and oxygen.

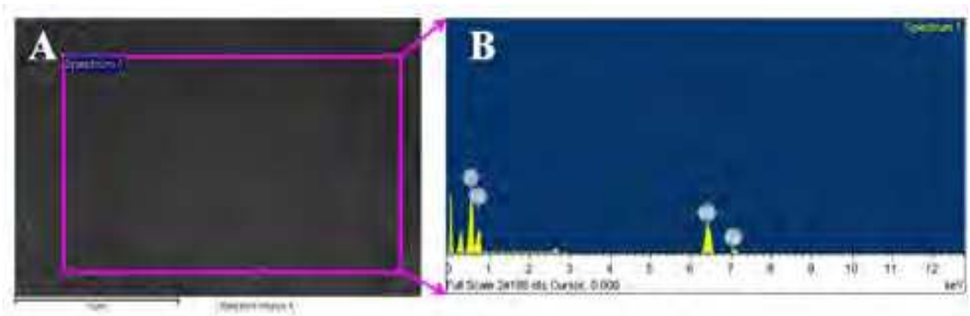

C

Element	Weight%	Atomic%
O K	45.89	74.75
Fe K	54.11	25.25
Totals	100.00	

Fig. 6. EDS of as-grown iron oxide NPs. (A) selected area, (B) EDS outcomes, and (C) elemental compositions (weight% and atomic%).

Transmission electron microscopy (**TEM**) is a microscopy technique whereby a beam of electrons is transmitted through an ultra thin specimen, interacting with the specimen as it passes through. An image is formed from the interaction of the electrons transmitted through the specimen; the image is magnified and focused onto an imaging device, such as a fluorescent screen, on a layer of photographic film, or to be detected by a sensor such as a CCD camera. TEMs are capable of imaging at a significantly higher resolution than light

microscopes, owing to the small de Broglie wavelength of electrons. This enables the instrument's user to examine fine detail-even as small as a single column of atoms, which is tens of thousands times smaller than the smallest resolvable object in a light microscope. TEM forms a major analysis method in a range of scientific fields, in both physical and biological sciences. TEMs find application in cancer research, virology, materials science as well as pollution and semiconductor research. At smaller magnifications TEM image contrast is due to absorption of electrons in the material, due to the thickness and composition of the material. At higher magnifications complex wave interactions modulate the intensity of the image, requiring expert analysis of observed images. Alternate modes of use allow for the TEM to observe modulations in chemical identity, crystal orientation, electronic structure and sample induced electron phase shift as well as the regular absorption based imaging. The first TEM was built by **Max Knoll** and **Ernst Ruska** in 1931, with this group developing the first TEM with resolving power greater than that of light in 1933 and the first commercial TEM in 1939.

High-resolution transmission electron microscopy (**HRTEM**) is an imaging mode of the transmission electron microscope (TEM) that allows the imaging of the crystallographic structure of a sample at an atomic scale (Spence, 1988). Because of its high resolution, it is an invaluable tool to study nanoscale properties of crystalline material such as semiconductors and metals. At present, the highest resolution realized is 0.8 angstroms (0.08 nm) with microscopes such as the OAM at NCEM. Ongoing research and development such as efforts in the framework of TEAM will soon push the resolution of HRTEM to 0.5 Å. At these small scales, individual atoms and crystalline defects can be imaged. Since all crystal structures are 3-dimensional, it may be necessary to combine several views of the crystal, taken from different angles, into a 3D map. This technique is called electron crystallography. One of the difficulties with HRTEM is that image formation relies on phase-contrast. In phase-contrast imaging, contrast is not necessarily intuitively interpretable as the image is influenced by strong aberrations of the imaging lenses in the microscope. One major aberration is caused by focus and astigmatism, which often can be estimated from the Fourier transform of the HR-TEM image.

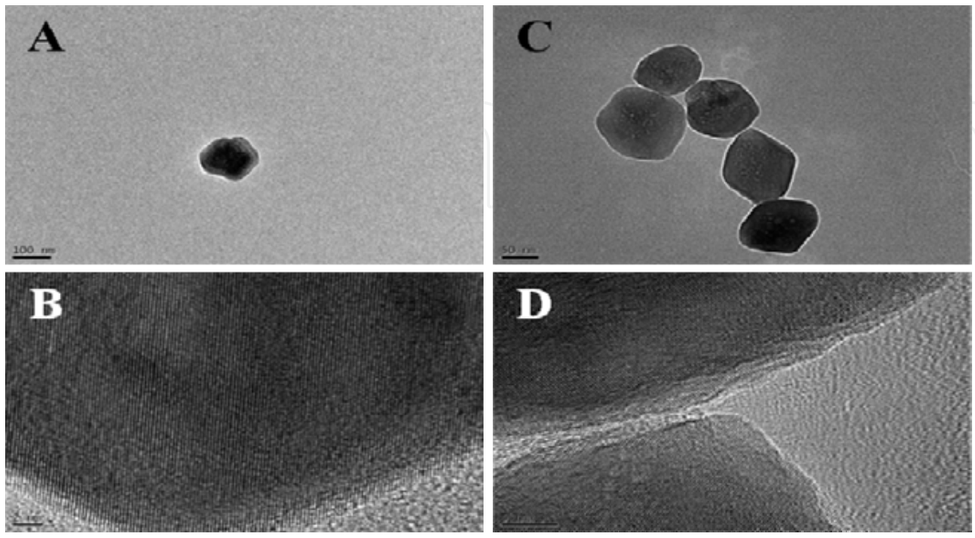

Fig. 7. (A and C)TEM and (B and D) HR-TEM images of iron oxide NPs

The morphologies of particles were observed by TEM, which are presented in the Fig. 7A and Fig. 7C. TEM photographs showed spherical NPs of iron oxide which appeared as deep dark spots. The diameter of as-grown iron oxide is in the range of 50 ~ 90 nm. A typical HR-TEM image of the iron NPs is shown in Figure 7B and 7D. It appears to be spherical in shape and fairly uniform in size with a mean diameter of 60 ± 10 nm. Most of the NPs are spherical in shape and the dimensions are well consistent with the FE-SEM observations. It is clearly revealed and calculated from the HR-TEM image that the distance between two lattice fringes is about 0.31 nm.

5. Potential applications of developed β-Fe_2O_3NPs

5.1 Photo-degradation of acridine orange (AO)

A **dye** can generally be described as a colored substance that has an affinity to the substrate to which it is being applied. The dye is generally applied in an aqueous solution, and may require a mordant to improve the fastness of the dye on the fiber. Both dyes and pigments appear to be colored because they absorb some wavelengths of light preferentially. In contrast with a dye, a pigment generally is insoluble, and has no affinity for the substrate. Some dyes can be precipitated with an inert salt to produce a lake pigment, and based on the salt used they could be aluminum lake, calcium lake or barium lake pigments. The first human-made (synthetic) organic dye, mauveine, was discovered by William Henry Perkin in 1856. Many thousands of synthetic dyes have since been prepared (Zollinger, 2003; Hunger, 2003). Synthetic dyes quickly replaced the traditional natural dyes. They cost less, they offered a vast range of new colors, and they imparted better properties to the dyed materials (Garfield, 2000). Dyes are now classified according to how they are used in the dyeing process.

Acridine orange is a nucleic acid selective fluorescent cationic dye useful for cell cycle determination. It is cell-permeable, and interacts with DNA and RNA by intercalation or electrostatic attractions respectively. When bound to DNA, it is very similar spectrally to fluorescein, with an excitation maximum at 502 nm and an emission maximum at 525 nm (green). When it associates with RNA, the excitation maximum shifts to 460 nm (blue) and the emission maximum shifts to 650 nm (red). Acridine orange will also enter acidic compartments such as lysosomes and become protonated and sequestered. In these low pH conditions, the dye will emit orange light when excited by blue light. Thus, acridine orange can be used to identify engulfed apoptotic cells, because it will fluoresce upon engulfment. The dye is often used in epifluorescence microscopy. Acridine orange is prepared from coal tar and creosote oil. Acridine orange can be used in conjunction with ethidium bromide to differentiate between viable, apoptotic and necrotic cells. Additionally, Acridine orange may be used on blood samples to fluoresce bacterial DNA, aiding in clinical diagnosis of bacterial infection once serum and debris have been filtered. Acridine orange can be used in the assessment of sperm chromatin quality.

Photodegradation is degradation of a photodegradable molecule caused by the absorption of photons, particularly those wavelengths found in sunlight, such as infrared radiation, visible light, and ultraviolet light. However, other forms of electromagnetic radiation can cause photodegradation. Photodegradation includes photodissociation, the breakup of molecules into smaller pieces by photons. It also includes the change of a molecule's shape to make it irreversibly altered, such as the denaturing of proteins, and the addition of other atoms or molecules. A common photodegradation reaction is oxidation. This type of

photodegradation is used by some drinking water and wastewater facilities to destroy pollutants. Photodegradation in the environment is part of the process by which ambergris evolves from its fatty precursor.

The molecular structure and absorbance spectra of AO are presented in the Figure 8A and 8B respectively. The photo-degradation of the AO dye occurs predominantly on the β-Fe_2O_3 NPs surface. The extent of degradation of the AO dye was measured by monitoring its concentration with and without NP after reaching the degradation. Figure 8C shows the gradual decreasing in absorption spectra for the degradation of AO dye as a function of photo-irradiation time. It is observed that the irradiation of an aqueous suspension of AO dye in the presence of iron oxide NP leads to decrease in absorption spectra at 491 nm.

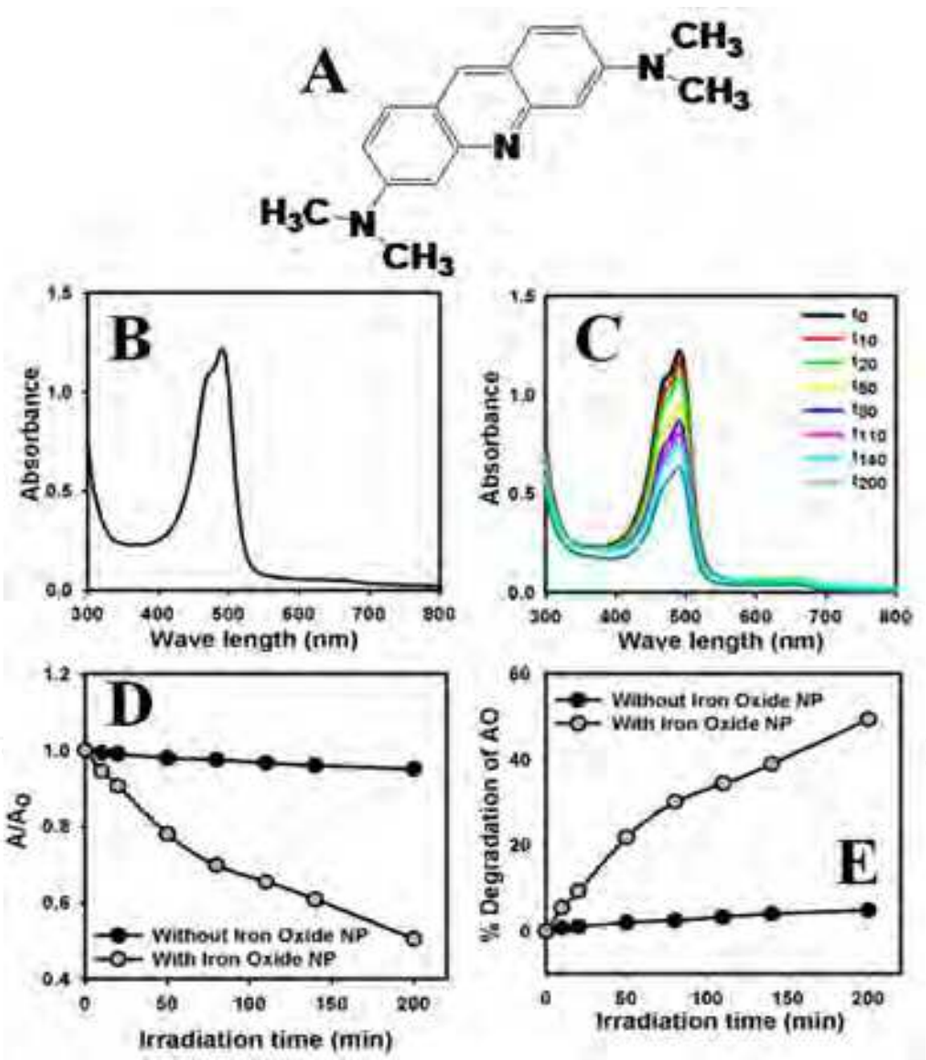

Fig. 8. Photocatalytic degradation of AO using iron oxide NPs. (A) Molecular structure of AO; (B) Spectrum of aqueous solution of AO; (C) Spectrum of AO at different time interval; (D) Change in absorbance; (E) % degradation in different time intervals of AO in presence and absence of as-grown iron oxide NPs.

The absorbance spectra at 491 nm is significantly decreased with increasing in exposure time and gradually decrease until 200 min which concludes that the AO dye has de-colorization property with iron oxide NPs close to 50%. The decrease in absorption intensity vs irradiation time for the AO in the presence and absence of iron oxide NPs is shown in the Figure 8D. Figure 8E shows a plot for the percent degradation versus irradiation time (min) for the oxygen saturated aqueous suspension of AO in the presence and absence of NPs. Figure 8E shows that around 50% degradation of the AO dye takes place after 200 min of irradiation in the presence of catalytic iron oxide NPs. The schematic representation of AO degradation is presented in Scheme 2.

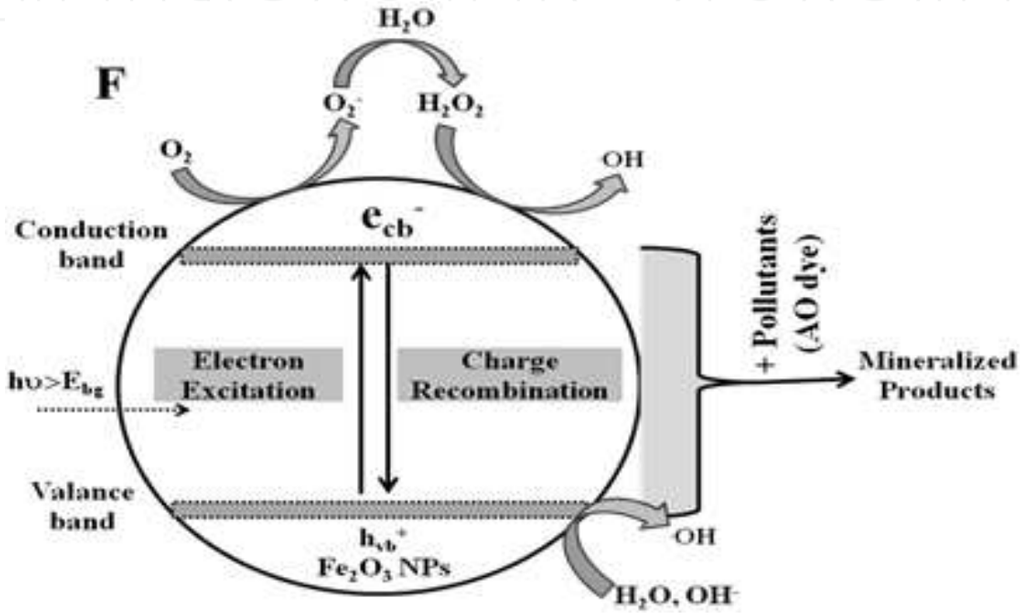

Scheme 2. Schematic representation of AO degradation mechanism

The experimental degradation rate constant is obtained from the initial slope acquired by linear regression from a plot of the natural logarithm (ln) of absorbance of the AO as a function of exposure time, i.e., first-order degradation kinetics. This rate constant is used to evaluate the degradation rates for the decomposition of AO using the formula appended below (vii):

$$-d[A]/dt = kc^n \quad \text{(vii)}$$

Where, k is the rate constant, c the concentration of the pollutant, and n the order of reaction. The rate of degradation is 9.9×10^{-5} mole.L^{-1}.Min^{-1}. The degradation of AO clearly demonstrated that prepared iron oxide (MO_x) NPs possess significant photocatalytic activity and these NPs could be beneficial photocatalysts for the removal of colored dyes.

Mechanism of heterogeneous photocatalysis has been discussed extensively in literature. When a semiconductor such as MO_x absorbs a photon of energy equal to or greater than its band gap, there will be the formation of electron/hole pair (**Scheme 2**). If charge separation is maintained, the electron and hole may migrate to the metal oxide surface, which can eventually bring about redox reactions of the organic substrates dissolved in water in the presence of oxygen. During the photo-catalytic oxidation processes hydroxyl radicals (·OH)

and superoxide radical anions ($O_2^{\cdot -}$) are supposed to be the main oxidizing species. These oxidative retorts would consequence in the mineralization of the dye.
Alternatively, direct absorption of light by the dye named AO, can lead to charge injection from the excited state of the AO to the conduction band of the semiconductor as summarized in the following equations (viii-xii):

$$MO_x + h\upsilon \rightarrow e^-_{cb} + h^+_{vb} \quad \text{(viii)}$$

$$O_2 + e^-_{cb} \rightarrow {}^{\cdot}O^-_2 \quad \text{(ix)}$$

$$H_2O + h^+_{vb} \rightarrow {}^{\cdot}OH + H^+ \quad \text{(x)}$$

$$AO_{ads} + h\upsilon \rightarrow AO_{ads}^* \quad \text{(xi)}$$

$$AO_{ads}^* + MO_x \rightarrow AO_{ads}^+ + {}^{\cdot}MO_2\,(e^-) \quad \text{(xii)}$$

The degradation process was initiated by the photolysis of MO_x-oxide/hydroxyl species, and accelerated by mercury beam irradiation, due to enhance photolysis of NPs species, which enhances the regeneration of metal precursor with concomitant production of oxide free radicals. Hydroxyl radicals ($OH^{\cdot}$) and superoxide radical anions ($O_2^{\cdot -}$) contribute to the oxidation process by attacking the dye molecules and would results in the bleaching of the AO dye. The results above clearly indicate that the prepared NPs shows a good photo-catalytic activity, thus it can be used as a photo-catalyst for the treatment of wastewater.

5.2 Chemical sensors

A **sensor** is a device that measures a physical quantity and converts it into a signal which can be read by an observer or by an instrument. For example, a mercury-in-glass thermometer converts the measured temperature into expansion and contraction of a liquid which can be read on a calibrated glass tube. A thermocouple converts temperature to an output voltage which can be read by a voltmeter. For accuracy, most sensors are calibrated against known standards. Nanotechnology can enable sensors to detect very small amounts of chemical vapors or liquids. Various types of detecting elements, such as semiconductor materials, carbon nanotubes, iron oxide nanoparticles, zinc oxide nanowires or palladium nanoparticles can be used in nanotechnology-based chemical sensors. These detecting elements change their electrical characteristics, such as resistance or capacitance, when they absorb a gas/liquid molecule on it. Because of the small size of nanoparticles/nanotubes/ nanowires, a few gas or liquid molecules are sufficient to change the electrical properties of the sensing elements. This allows the detection of a very low concentration of chemical vapors or liquids. This goal is to have small, inexpensive sensors that can sniff out chemicals just as dogs are used in airports to smell the vapors given off by explosives or drugs. The capability of producing small, inexpensive sensors that can quickly identify chemicals provides a king of nano-bloodhound that doesn't need sleep or exercise which can be useful in a number of ways. An obvious application is to mount these sensors throughout an airport, or any facility with security concerns, to check for vapors given off by explosive devices.
The potential application of β-Fe_2O_3 nanoparticles as chemical sensors has been explored for detecting and quantifying hazardous chemicals, which are not environmental friendly as well as safe. Development of this nanostructure material as chemi-sensors is in the primitive

stage. The β-Fe_2O_3 NPs chemi-sensors have advantages such as stability in air, non-toxicity, chemical stability, electrochemical activity, ease to fabricate, and bio-safe characteristics. As in the case of chemical sensors, the principle of operation is that the current response in I-V technique of β-Fe_2O_3 NPs drastically changes when aqueous ammonia are adsorbed. The β-Fe_2O_3 nano-materials were used for fabrication of chemical sensor, where aqueous ammonia was considered as target analyte. The emaciated-film of nanomaterials sensor were fabricated with conducting agents and embedded on the gold electrode surface, which is presented in the Scheme 3(A). The fabricated electrode was accumulated in the oven at low temperature (60.0 °C) for 2 hours to dry, stable, and uniforms the film totally. The electrical responses of target analyte were executed using I-V method, which is presented in Scheme 3(B). Hypothetical, experimental, and mechanism of I-V responses of chemical sensor having β-Fe_2O_3 NPs thin film as a function of current versus potential for aqueous ammonia, which is shown in Scheme 3(B), Scheme 3(C), and Scheme 3(D) respectively. The time delaying of electrometer was kept for 1.0 sec. A significant increase in the current value with applied potential is clearly demonstrated.

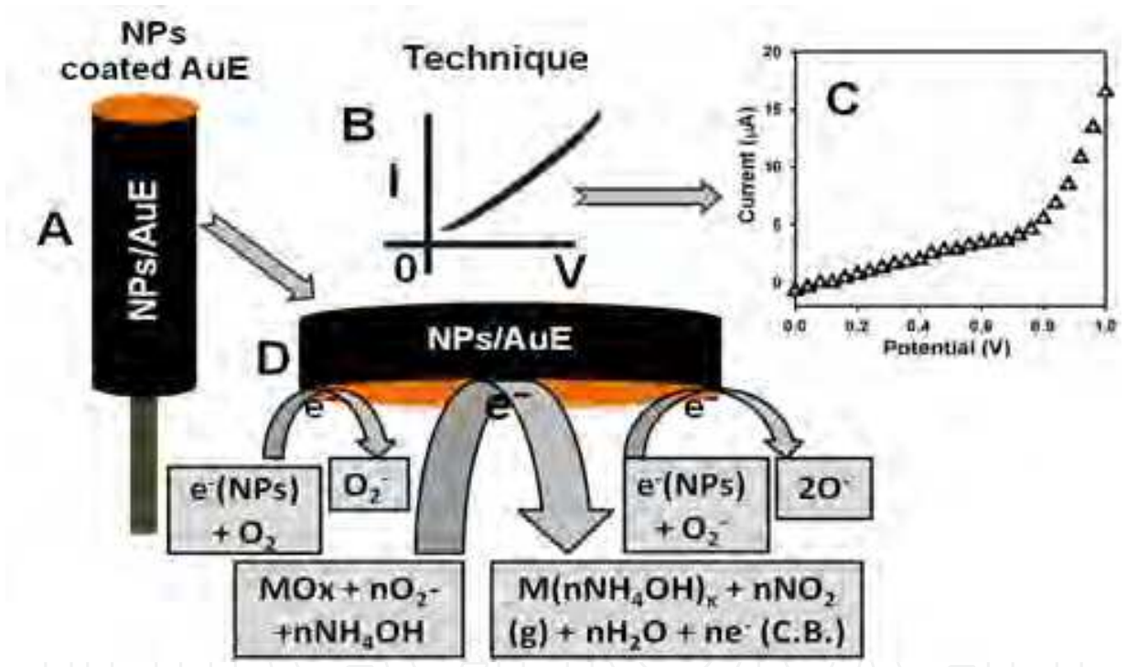

Scheme 3. Schematic view of (A) fabrication of AuE with β-Fe_2O_3 NPs and coating agents, (B) detection I-V method (theoretical), (C) experimental result of I-V plot, (D) proposed mechanisms of aqueous ammonia detection in presence of semiconductor β-Fe_2O_3 nanomaterials.

I-V responses of chemical sensor having β-Fe_2O_3 thin film as a function of current versus potential for the liquid ammonia, which is exposed in Figure 9. A significant increase in the current value with applied potential is clearly demonstrated, where the time delaying for electrometer is kept 1.0 sec. Fig. 9A represents the current changing before (dark-dotted) and after (gray-dotted) coating was made with NPs on gold electrode. The gray-dotted and dark-dotted curves indicated the response of the film before and after injecting 100.0 μl chemicals in bulk solution respectively, which is presented in Fig. 9B. Significant increase of

surface film current is measured after every injection of the target component. 77.0 μM concentration of aqueous ammonia is initially taken into the electrochemical cell and added the higher concentration (10 times) in each injection from the stock analyte solution. During I-V measurement, it is injected low to high analyte concentrations (77.0 μM to 7.7 M) gradually into the 20.0 ml phosphate buffer solution in every step. Each I-V response to varying concentration of aqueous ammonia from 7.7 M to 77.0 μM on thin iron oxide NPs coating is presented in the Fig. 9C. It shows the current response changed of the iron oxide NPs as a function of ammonium hydroxide concentration in room conditions. It is observed that at lower to higher concentration of target compound, the current increase gradually. A wide range of analyte concentration was preferred to study the possible analytical parameters, which is calculated in 77.0 μM to 0.77 M. The calibration curve is plotted from the variation of analyte concentrations, which is revealed in the Fig. 9D. The sensitivity is calculated from the calibration curve, which is close to 0.5305 ± 0.02 $\mu Acm^{-2}mM^{-1}$. The linear dynamic range of this sensor exhibits from 77.0 μM to 0.77 M and the detection limit was around 21.8 ± 0.1 μM [3×noise(N)/slope(S)].

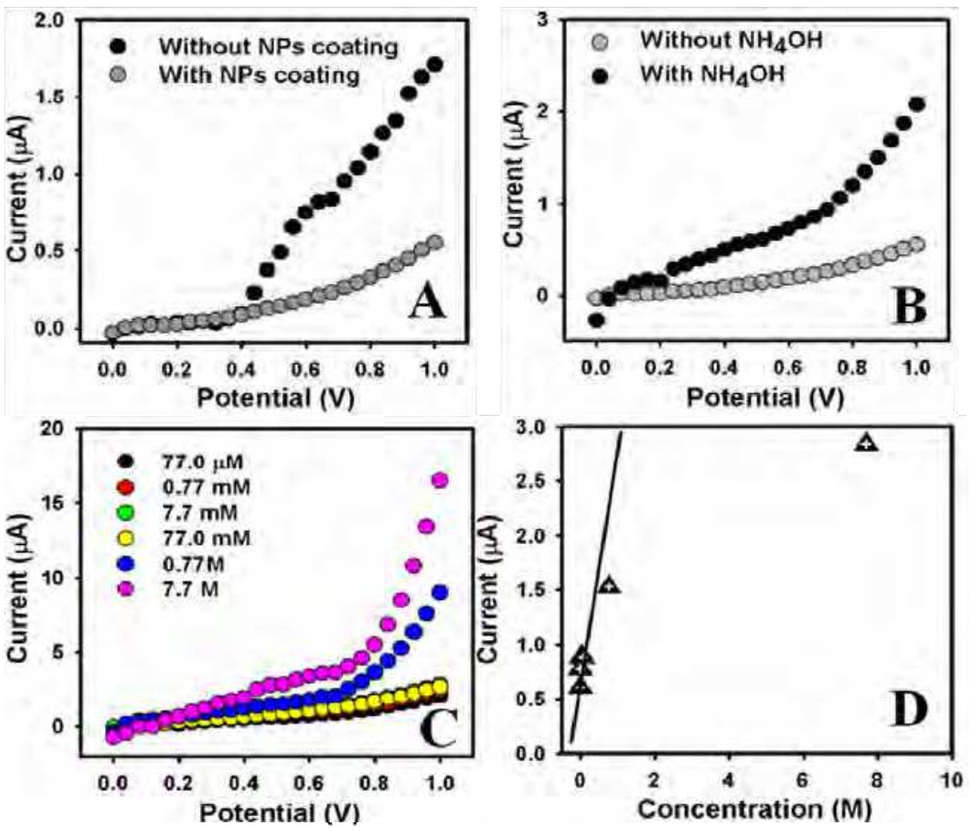

Fig. 9. I-V curves of (A) with and without coating of NPs; (B) with and without ammonium hydroxide (77.0 μM) using NPs coated gold electrode; (C) Concentration variation of ammonium hydroxide; and (D) calibration curve of ammonium hydroxide sensors

The response time was around 10.0 sec for the NPs coated-electrode to reach saturated steady state current. The high sensitivity of film can be attributed to the good absorption (porous surfaces fabricated with coating) and adsorption ability, high catalytic activity, and

good biocompatibility of the iron oxide NPs. The estimated sensitivity of the fabricated sensor is relatively higher than previously reported ammonium hydroxide sensors based on other composite or materials modified electrodes (Raj et al., 2010). The aqueous ammonia sensing method of β-Fe_2O_3 NPs sensor is based on the semiconductor oxides, due to oxidation or reduction of the metal-oxide itself, in accordance with the dissolved oxygen (O_2) in bulk-solution or surface-air of the surrounding atmosphere (Scheme 4A), according to the equations (xiii-xiv).

$$\text{electron } (e^-, \beta\text{-}Fe_2O_3 \text{ NPs}) + O_2 \rightarrow O_2^- \quad \text{(xiii)}$$

$$\text{electron } (e^-, \beta\text{-}Fe_2O_3 \text{ NPs}) + O_2^- \rightarrow 2O^- \quad \text{(xiv)}$$

These reactions take place in bulk-solution or air/liquid interface or surrounding air due to the low carrier concentration which increased the resistances. The aqueous ammonia sensitivity headed to β-Fe_2O_3 NPs (i.e. MO_x) could be attributed to the high oxygen deficiency and defect density leads to increase oxygen adsorption. Larger the amount of oxygen adsorbed on the MO_x NPs surfaces, larger would be the oxidizing capability and faster would be the oxidation of analytes.

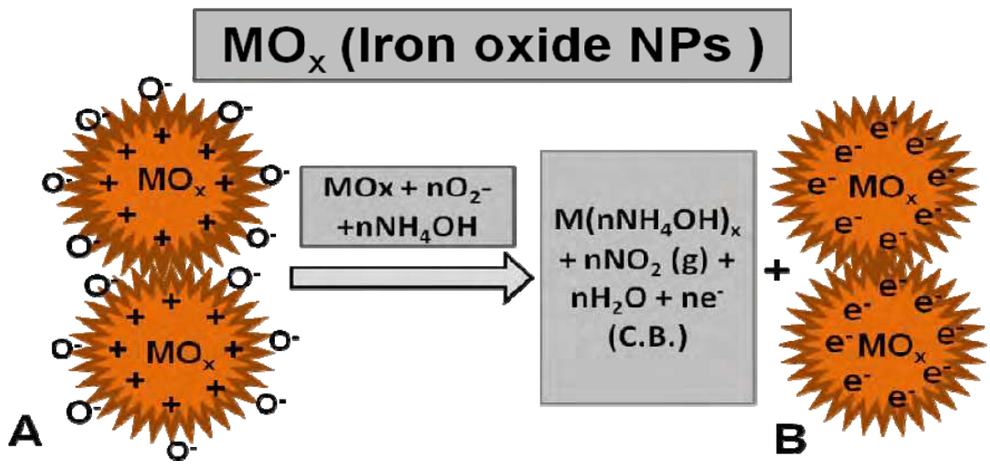

Scheme 4. Mechanism of β-Fe_2O_3 NPs chemical sensors at room conditions.

The reactivity of aqueous ammonia would be very large as compared and contrasted to other chemical with the semiconductor surfaces under the similar condition (Patil et al., 2007). When NH_4OH reacts with the adsorbed oxygen on the surface of the film, it acquires oxidized to nitrogen oxide gas and metal ammonium hydroxide, liberating free electrons in the conduction band (Scheme 4B), which could be articulated through the following reactions (xv-xvi):

$$MO_x + nNH_4OH + nO_2^- \rightarrow M(nNH_4OH)x + nNO_2\,(g) + nH_2O + ne^-\,(C.B.) \quad \text{(xv)}$$

$$4NH_4OH + 7O_2^- \rightarrow 4NO_2 + 10H_2O + 15e^- \quad \text{(xvi)}$$

These reactions corresponded to oxidation of the reducing carriers. These processes increased the carrier concentration and hence decreased the resistance on exposure to reducing liquids/analytes. At the room condition, the disclosure of metal oxide surface to

reducing liquid/analytes results in a surface mediated combustion process. The exclusion of iono-sorbed oxygen amplifies the electron concentration and thus the surface conductance of the coating-film (Mujumdar, 2009). The reducing analyte (aq. NH_3) donates electrons to β-Fe_2O_3 NPs surface. Therefore, resistance is decreased, or conductance is increased. This is the reason why the analyte response (current response) increases with increasing potential. On the other way, due to large surface area, the NPs of provide a supportive nano-environment for the chemical detection with fast and good capacity. The high sensitivity of NPs provides high electron communication features which progress the direct electron movement between the active sites of NPs and GE. The modified thin film had a good stability and reproducibility. As for the nanomaterials, β-Fe_2O_3 NPs provide a path to a new generation of chemical sensors, but a premeditate effort has to be expended for nanostructures to be taken critically for large scale applications, and to achieving high appliance density with accessibility to individual sensors. Reliable methods for fabricating, assembling and integrating building blocks onto sensors need to be explored.

6. Conclusion

Finally, the present work provides a hydrothermal method to synthesize low-dimensional iron oxide NPs, which was characterized using several conventional techniques like XRD, FE-SEM, EDS, HR-TEM, UV/visible, FT-IR, and Raman spectroscopy. The detailed morphological characterizations by FE-SEM and TEM revealed that the synthesized NPs possess almost spherical shape with typical diameters of ~ 60 ± 10 nm. The optical properties of as-grown β-Fe_2O_3 NPs were investigated by UV-visible absorption which shows the presence of characteristic β-Fe_2O_3 peak in the spectrum. It was also investigated the photo-catalytic degradation with Acridine orange under UV radiation sources and found the 50% degradation held with as-grown β-Fe_2O_3 NPs. The as-grown NPs were employed for the detection of aqueous ammonia in solution phase as chemical sensors. The performance of the proposed aqueous ammonia sensor using low-dimensional β-Fe_2O_3 NPs film was excellent in terms of sensitivity, lower detection limit, and large linear dynamic ranges in short response time. This new approach is also introduced a new route for efficient chemical sensor development to control the environmental toxicity as well as carcinogenicity, and can also play an important role in environmental and health care fields.

7. Acknowledgment

We are greatly acknowledged to Najran University for their financial supports and research facilities. Centre for Advanced Materials and Nano-Engineering (CAMNE), Najran University, Najran is also greatly acknowledged for their chemicals and nanomaterials analyses.

8. References

Ansari, SG., Ansari, ZA., Wahab, R., Kim, YS., Khang, G., Shin, HS. (2008). Glucose sensor based on nano-baskets of tin oxide templated in porous alumina by plasma enhanced CVD. *Biosens. Bioelectron*. Vol. 23, pp. 1838.

Azároff, L. V.; R. Kaplow, N. Kato, R. J. Weiss, A. J. C. Wilson, R. A. Young (1974). X-ray diffraction. McGraw-Hill.

Ballun, G., Hajdu, F., Harsanyi, G. (2003). Highly sensitive ammonia sensor. IEEE 26th Int. Spring Sem. *Elect. Tech*. pp. 471.

Buzea, C., Pacheco, I., Robbie, K. (2007). "Nanomaterials and Nanoparticles: Sources and Toxicity". *Biointerphases* Vol. 2, pp. MR17.

Brown, ASC., Hargreaves, JSJ., Rijniersce, B. (1998) A study of the structural and catalytic effects of sulfation on iron oxide catalysts prepared from goethite and ferrihydrite precursors for methane oxidation. *Catal. Lett*. Vol. 53, pp. 7.

Chen, J., Xu, LN., Li, WY., Gou, Xl. (2005) α-Fe_2O_3 Nanotubes in Gas Sensor and Lithium-Ion Battery Applications. *Adv. Mater*. Vol. 17, pp. 582.

Cherepy, NJ., Liston, DB., Lovejoy, JA., Deng, H., Zhang, ZJ. (1998). Ultrafast Studies of Photoexcited Electron Dynamics in γ- and α-Fe_2O_3 Semiconductor Nanoparticles. *J. Phys. Chem. B* Vol. 102, pp. 770.

Compendium of Chemical Terminology, 2nd ed. (1997) the "Gold Book". Online corrected version: (2006).

Cornell, RM., Schwertmann, U. (2003) *The Iron Oxides-Structure, Properties, Reactions, Occurrences and Uses*. Darmstadt: Wiley–VCH GmbH & Co. KGaA.

Cornell, RM., Schwertmann, U. (2003). *The iron oxides: structure, properties, reactions, occurrences and uses*. Wiley VCH.

Christie, S., Scorsone, E., Persaud, K., Kvasnik, F. (2003). Remote detection of gaseous ammonia using the near infrared transmission properties of polyaniline. *Sens. Actuators B* Vol. 90, pp. 163.

Dale, L., Huber. (2009) Synthesis, Properties, and Applications of iron NPs. *Small*. Vol. 1, pp. 482.

Fahlman, BD. (2007). *Materials Chemistry*. Springer. pp. 282.

Kumar, A., Singhal, A. (2007) Synthesis of colloidal β-Fe_2O_3 nanostructures—influence of addition of Co^{2+} on their morphology and magnetic behavior. *Nanotechn.* Vol. 18, pp. 475703.

Garcıa, KE., Morales, AL., Barrero, CE., Arroyave, CE., Greneche, JM. (2004) Magnetic and crystal structure in akaganeite nanoparticle. *Physica B*. Vol. 354, pp. 187.

Hunger, K., ed. (2003). Industrial Dyes. Chemistry, Properties, Applications. Weinheim: Wiley-VCH.

Garfield, S. (2000). *Mauve: How One Man Invented a Color That Changed the World*. Faber and Faber. ISBN 0-393-02005-3.

Jordan, A., Scholz, R., Maier-Hauff, K., Johannsen, M., Wust, P., Nadobny, J., Schirra, H., Schmidt, H., Galatsis, K., Cukrov, L., Wlodarski, W., McCormick, P., Kalantar-zadeh, K., Comini, E., Sberveglieri, G. (2003) p- and n-type Fe-doped SnO_2 gas sensors fabricated by the mechanochemical processing technique. *Sens. Actuators B*. Vol. 93, pp. 562.

Kesavan, V., Sivanand, Chandrasekaran, PSS., Koltypin, Y., Gedanken, A. (1999) Catalytic aerobic oxidation of cycloalkanes with nanostructured amorphous metals and alloys. *Angew. Chem. Int. Ed*. Vol. 38, pp. 3521.

Long, GL., Winefordner, JD. (1983). Linearization of electron capture detector response to strongly responding compounds. *Anal. Chem*. Vol. 55, pp. 713.

MacDougall, D., Crummett, WB. (1980). Guidelines for Data Acquisition and Data Quality Evaluation in Environmental Chemistry. *Anal. Chem*. Vol. 52, pp. 2242.

McMichael, RD., Shull, RD., Swartzendruber, LJ., Bennett, LH. (1992) Magnetocaloric effect in superparamagnets. *J. Magn. Magn. Mater*. Vol. 111, pp. 29.

Mujumdar, S. (2009). Synthesis and characterisation of SnO_2 films obtained by a wet chemical process. *Mat. Sci. Poland*. Vol. 27, pp. 123.

Music, S., Saric, A., Popovic, S. (1997) Effect of urotropin on the formation of β-FeOOH. *J. Mol. Struct.* Vol. 410–411, pp. 153.

O'Donoghue, M. (1983). A guide to Man-made Gemstones. *Great Britain: Van Nostrand Reinhold Company*. pp. 40.

Patil, DR., Patil, LA., Amalnerkar, PP. (2007). Ethanol gas sensing properties of Al_2O_3-doped ZnO thick film resistors. *Bull. Mat. Sci*. Vol. 30, pp. 553.

Pare, B., Jonnalagadd, SB., Tomar, H., Singh, P., Bhagwat, BW. (2008). ZnO assisted photocatalytic degradation of acridine orange in aqueous solution using visible irradiation. *Desalination* Vol. 232, pp. 80.

Raj, VB., Nimal, AT., Parmar, Y., Sharma, MU., Sreenivas, K., Gupta, V. (2010). Cross-sensitivity and selectivity studies on ZnO surface acoustic wave ammonia sensor. *Sens. Actuators B* Vol. 147, pp. 517.

Raj, K., Moskowitz, B., Casciari, R. (1995) Advances in ferrofluid technology. *J. Magn. Magn. Mater.* Vol. 149, pp. 174.

Rahman, MM., Jamal, A., Khan, SB., Faisal. M. (2011) Fabrication of Highly Sensitive Ethanol Chemical Sensor Based on Sm-Doped Co_3O_4 Nano-Kernel by Solution Method. J. Phys. Chem. C. Vol. 115 pp. 9503.

Rahman, MM., Jamal, A., Khan, SB., Faisal. M. (2011) Cu-doped ZnO Based Nanostructured Materials for Sensitive Chemical Sensor Applications. ACS App. Mater. Inter. Vol. 3 pp. 1346

Rahman, MM., Umar, A., Sawada, K. (2009) Development of Amperometric Glucose Biosensor Based on Glucose Oxidase Enzyme Immobilized with Multi-Walled Carbon Nanotubes at Low Potential Sens. Actuator: B Vol. 137 pp. 327.

Rahman, MM., Jeon, IC., Hasnat, MA., Samed, AJF. (2006) Xenon Beam Radiation Assisted Degradation of an Organic dye in Aqueous Medium. *Environ. Sci. Technol*. Vol. 1 pp. 210.

Saquib, M., Tariq, MA., Faisal, M., Muneer, M. (2008). Photocatalytic degradation of two selected dye derivatives in aqueous suspensions of titanium dioxide. Desalination. *Desalination* Vol. 219, pp.301.

Spence, JCH. (1988) [1980]. *Experimental high-resolution electron microscopy*. New York: Oxford U. Press. ISBN 0195054059.

Whitesides, GM., Boncheva, M. (2002) Beyond molecules: Self-assembly of mesoscopic and macroscopic components. *Proc. Natl. Acad. Sci. USA*. Vol. 99, pp. 4769.

Zeng, H., Li, J., Liu, JP., Wang, ZP., Sun, SH. (2002). Exchanged-coupled nanocomposite magnets via nanoparticle self-assembly. *Nature* Vol. 420, pp. 395.

Zollinger, H. 3rd ed. (2003). *Color Chemistry. Synthesis, Properties and Applications of Organic Dyes and Pigments*, Weinheim: Wiley-VCH.

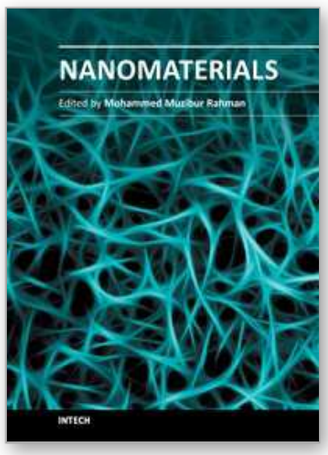

Nanomaterials

Edited by Prof. Mohammed Rahman

ISBN 978-953-307-913-4
Hard cover, 346 pages
Publisher InTech
Published online 22, December, 2011
Published in print edition December, 2011

The book "Nanomaterials" includes all aspects of metal-oxide nano-structures, nano-composites, and polymer materials instigating with materials survey and preparations, growth and characterizations, processing and fabrications, developments and potential applications. These topics have utilized innovative methods of preparation, improvement, and continuous changes in multidimensional ways. The innovative frontiers are branching out from time to time to advanced nanotechnology. It is an important booklet for scientific organizations, governmental research-centers, academic libraries, and the overall research and development of nano-materials in general. It has been created for widespread audience with diverse backgrounds and education.

How to reference

In order to correctly reference this scholarly work, feel free to copy and paste the following:

Mohammed M. Rahman, Sher Bahadar Khan, Aslam Jamal, Mohd Faisal and Abdullah M. Aisiri (2011). Iron Oxide Nanoparticles, Nanomaterials, Prof. Mohammed Rahman (Ed.), ISBN: 978-953-307-913-4, InTech, Available from: http://www.intechopen.com/books/nanomaterials/iron-oxide-nanoparticles

INTECH
open science | open minds

InTech Europe
University Campus STeP Ri
Slavka Krautzeka 83/A
51000 Rijeka, Croatia
Phone: +385 (51) 770 447
Fax: +385 (51) 686 166
www.intechopen.com

InTech China
Unit 405, Office Block, Hotel Equatorial Shanghai
No.65, Yan An Road (West), Shanghai, 200040, China
中国上海市延安西路65号上海国际贵都大饭店办公楼405单元
Phone: +86-21-62489820
Fax: +86-21-62489821

IntechOpen